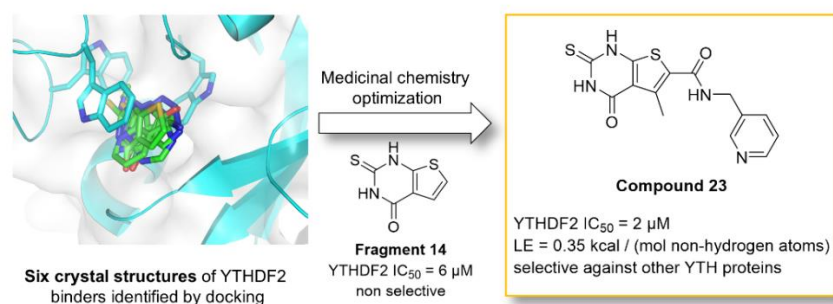


# Discovery of YTHDF2 ligands by fragment-based design

Annalisa Invernizzi, Francesco Nai, Rajiv Kumar Bedi, Pablo Andrés Vargas-Rosales, Yaozong Li, Elena Bochenkova, Marcin Herok, František Zálešák, Amedeo Caflisch\*

Department of Biochemistry, University of Zurich, CH-8057 Zurich. Switzerland

**KEYWORDS:** epitranscriptomics, m<sup>6</sup>A readers, YTH proteins, docking, structure-activity relationship, HTRF binding assay, FP binding assay, molecular dynamics, protein crystallography



**ABSTRACT:** N<sup>6</sup>-Adenosine methylation is the most abundant modification of mRNA. The three members of the YTH domain family proteins (YTHDF1-3) recognize in the cytoplasm the m<sup>6</sup>A-RNA modification. We carried out a screening campaign by fragment-based high-throughput docking into YTHDF2 that resulted in the identification of six ligands with a hit rate of 13%. The acquisition of 28 analogues of the docking hits provided an additional set of 10 active compounds (IC<sub>50</sub> < 100 μM). Further optimization of a ligand-efficient fragment by the synthesis of 32 derivatives culminated in a series of YTHDF2 ligands which show low-micromolar affinity measured by a fluorescence-polarization (FP) assay and a homogeneous time-resolved fluorescence-based (HTRF) assay. The series is characterized by very favorable ligand efficiency (of about 0.3 – 0.4 kcal/mol per non-hydrogen atom). Compound **23** binds to YTHDF2 according to the FP and HTRF assays with IC<sub>50</sub> values of 2 μM and 10 μM, respectively, and it is selective against all the other YTH reader proteins. Several compounds of the series bind to the three YTHDF proteins with similar low-micromolar affinity, while they are less potent for YTHDC1 and YTHDC2. In contrast, compounds **17** and **30** bind also to YTHDC2, with affinity of 9 μM and 7 μM, respectively. We also disclose six crystal structures of YTHDF2 in the complex with the fragments identified by docking.

## Introduction

The YTH (YT521-B homology) domain-containing proteins are a family of RNA-binding proteins that specifically recognize N<sup>6</sup>-methyladenosine (m<sup>6</sup>A), the most abundant internal modification in eukaryotic RNA.<sup>1</sup> These proteins play critical roles in various biological processes, including mRNA metabolism, splicing, stability, and translation, influencing gene expression and cellular functions.<sup>1-3</sup> The YTH family consists of five members: YTHDF1 (from now on referred to as DF1), YTHDF2 (DF2), YTHDF3 (DF3), YTHDC1 (DC1), and YTHDC2 (DC2).<sup>4</sup> DC1 is primarily nuclear, where it participates in mRNA splicing, processing, and export.<sup>5</sup> In contrast, the DF proteins (DF1, DF2, and DF3) are mainly cytoplasmic and play essential roles in mRNA translation, stability, and degradation.<sup>3</sup> Finally, DC2 is the latest discovered member of this protein family and is mostly cytoplasmic, even though it has been found to interact with nuclear components, suggesting a dual role in RNA processing

and regulation.<sup>6,7</sup> Its functions appear to overlap with those of DF proteins, particularly in regulating RNA translation and stability. While other family members are broadly expressed across various cell types, DC2 is notably enriched in the testes, where it plays a critical role in germ cell development and maturation.<sup>6</sup>

While it has been established that each YTH protein possesses unique functions, there is evidence indicating that they can compensate for one another under certain conditions, leading to functional redundancy.<sup>4,8,9</sup> Research has demonstrated that the DF proteins can engage in context-dependent functional compensation. For instance, when one DF protein is knocked down, the others can partially compensate for the loss, maintaining the overall regulation of mRNA metabolism.<sup>8,9</sup> This phenomenon highlights the complexity of the YTH protein family, where the precise roles of individual members may vary depending on the cellular context, the specific mRNA targets, and the presence of other regulatory factors.<sup>4,8,9</sup>

Given their crucial role in gene expression regulation, it is not surprising that YTH proteins and m<sup>6</sup>A regulation are heavily implicated in various diseases, especially cancer. Our study focuses on DF2, which is involved in multiple types of cancer including prostate cancer,<sup>10</sup> MYC-driven breast cancer,<sup>11</sup> and acute myeloid leukemia (AML).<sup>12</sup> This makes DF2 a highly attractive target for drug discovery, which is gaining more and more attention. Even though we focus mainly on DF2, the highly conserved m<sup>6</sup>A binding site of the DF proteins hinders the development of a DF2 selective ligand.<sup>13</sup> Furthermore, the discussed compensatory effects make a pan-DF ligand desirable.

Only a few small-molecule ligands have been identified for the DF protein family. Among them are Ebselen,<sup>14</sup> Tegaserod,<sup>15</sup> and Salvianolic Acid C,<sup>16</sup> previously known compounds repurposed from other targets. Reviews of known inhibitors of the YTH-proteins can be found in Refs.<sup>17,18</sup> In our earlier publication,<sup>13</sup> we reported the first small molecules binders of DF2; the X-ray crystal structure of one of them (compound **11**, IC<sub>50</sub> = 174 μM)<sup>13</sup> is the starting point of this work. Subsequently, Wang et al. reported the discovery of DC-Y13-27, a DF2 inhibitor with an IC<sub>50</sub> of 21.8 μM (measured using an AlphaScreen assay) and a K<sub>d</sub> of 38 μM (determined by microscale thermophoresis).<sup>19</sup> The compound showed weaker activity on DF1 (IC<sub>50</sub> = 165 μM in the AlphaScreen assay), but was not tested on DF3.<sup>19</sup> A more recent study identified a series of functionalized pyrazoles as selective DF2 binders.<sup>20</sup> The most potent compound, CK-75, exhibited an IC<sub>50</sub> of 13.2 μM in an AlphaScreen assay and was found to be inactive against all other members of the YTH protein family. Notably, CK-75 induced cell cycle arrest and apoptosis in the K567 leukemia cell line, further supporting DF2 as a promising therapeutic target.<sup>20</sup>

Here we present a new series of DF2 binders identified by docking followed by SAR-by-catalog. We discovered new chemotypes that compete with m<sup>6</sup>A-RNA for binding to DF2. Medicinal chemistry optimization of a ligand-efficient scaffold resulted in a series of low-micromolar binders of DF2. Most compounds of the series show a preference for the DF proteins against DC1 and DC2. Compound **23** binds only to DF2, being selective against all the other YTH proteins.

## Results and discussion

### High-throughput docking

To find new small-molecule binders of DF2 we started with a high-throughput docking campaign. A library of 500,000 fragments was docked using the program SEED.<sup>21,22</sup> The fragments were selected from the ZINC20 database<sup>23</sup> according to the following rules: between 11 and 20 heavy atoms, at least one ring, and at least one sp<sup>3</sup>-hybridized carbon. For each of the extracted compounds, up to 20 conformers were generated using a distance geometry-based algorithm,<sup>24</sup> and docked by SEED. Two structures of the m<sup>6</sup>A-RNA recognition domain of DF2 were used for docking (Figure 1). The crystal structure in the complex with 6-cyclopropylpyrimidine-2,4-diol (compound **11** in Ref.<sup>13</sup>, PDB ID: 7R5W) and a snapshot obtained by molecular dynamics (MD) simulations started from the same crystal structure. The MD snapshot was selected by analysis of

the time series of the volume of the recognition pocket. It has a more open recognition loop<sup>25</sup> with a pocket volume of 600 Å<sup>3</sup> which is significantly larger than the volume of 324 Å<sup>3</sup> in the crystal structure 7R5W (Figure 1).

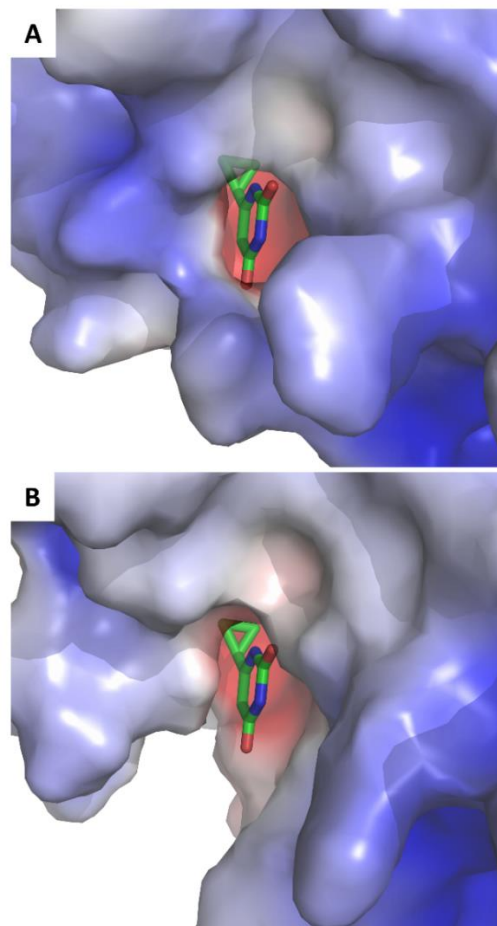


**Figure 1.** The two structures of the DF2 reader employed for docking. (a) X-ray crystal structure of DF2 in the complex with 6-cyclopropylpyrimidine-2,4-diol (compound **11** of Ref.<sup>13</sup>, PDB: 7R5W). (b) MD-simulation snapshot with larger aperture of the m<sup>6</sup>A-recognition pocket (see Methods). The surface of DF2 is colored by electrostatic potential (red, negative; blue, positive).

The two protein structures were kept rigid during docking and evaluation of the binding energy. SEED calculates the binding energy by a force field with implicit treatment of the electrostatics effects of the solvent. The docked compounds were ranked according to two energy terms, namely the total binding energy, and the difference between the electrostatic contribution to the intermolecular interaction energy in the solvent and the solvation energy of the ligand. The top-scoring compounds were then selected if they showed the crucial hydrogen bond with the backbone carbonyl of C433 which is the acceptor of the N6 of the natural ligand m<sup>6</sup>A. If an interesting compound was not commercially available, a structurally similar analogue was chosen. Finally, 25 and 22 compounds were selected from the docking campaigns that made use of the crystal structure and MD snapshot, respectively (Table S1). Fragment screening

by SEED requires about 1 s per fragment. SEED is available as an open-source code from GitLab (<https://gitlab.com/CaflischLab>).

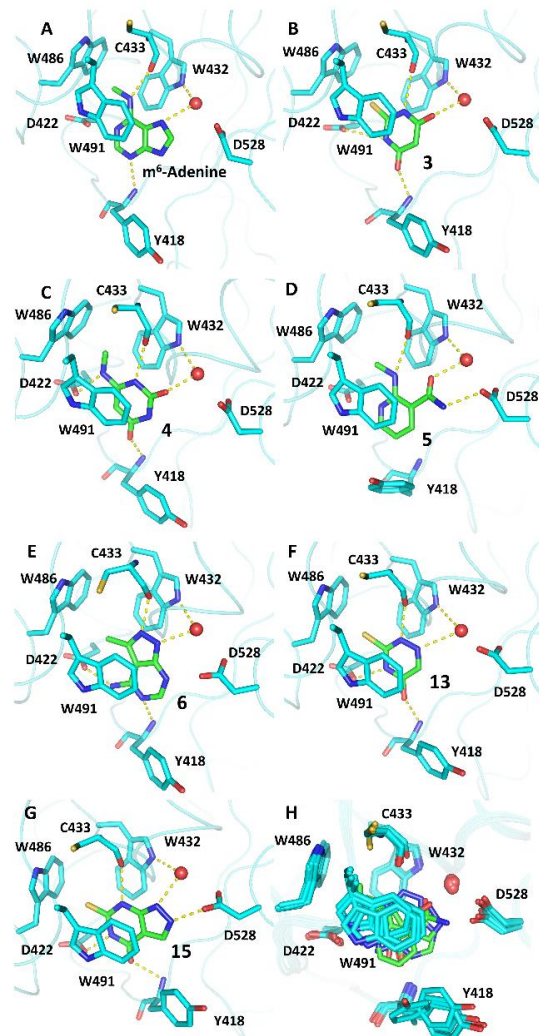
### In vitro validation

A previously reported homogeneous time-resolved fluorescence (HTRF)-based assay was used to measure the binding affinity of the 47 ordered compounds (see Methods).<sup>26</sup> For the 9 compounds with residual signal at 1 mM smaller than 60% (with respect to DMSO control) the IC<sub>50</sub> value was determined by dose-response experiments (Table S1). Among these, the thiobarbiturate derivatives **1** and **2** were the strongest binders, with IC<sub>50</sub> values of 19 μM and 170 μM, respectively (Table 1). The X-ray crystal structure was solved for compounds **3-6** at high resolution (Table 1, Figure 2b-e). The six binders **1-6** (Table 1) belong to four distinct chemotypes: thiobarbiturates (**1-3**), uracil (**4**), nicotinamide (**5**), and pyrazolopyrimidine (**6**). The thiobarbiturate derivative **1** shows a very favorable LE of 0.50 while the toluene group of compound **2** does not seem to contribute to binding. Compounds **3**, **4**, and **6** also maintain the interaction with the backbone NH of Y418, and additionally, they can form an H-bond with the side chain of D422. This new interaction may offer selectivity against the nuclear reader DC1, which features the N367 hydrogen bond donor NH<sub>2</sub> in this position.<sup>27</sup> In our earlier publication<sup>13</sup>, we described a series of uracil analogues; compound **4**, is a new member of this series with a modest IC<sub>50</sub> value of 246 μM. The amide nitrogen atom of compound **5** is involved in a hydrogen bond with the side chain of D528, but it does not form favorable interactions with D422 and the backbone NH of Y418. The 70° relative orientation and 4.8 Å distance between the ring centers indicate that the aromatic side chain of Y418 engages in an edge-to-face π-stacking interaction with **5**.<sup>28,29</sup>

### SAR by catalogue

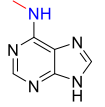
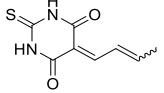
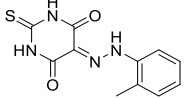
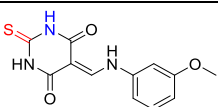
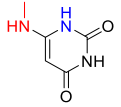
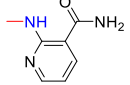
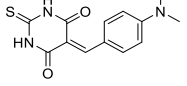
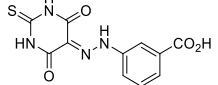
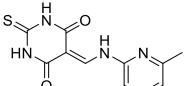
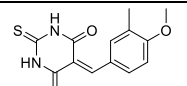
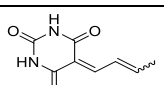
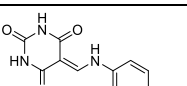
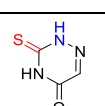
From the information gained in the first screening, a second set of 28 compounds was ordered (Table S2). This set consisted of 14 top-ranking docked molecules with chemotype similar to the one of compounds **1-3**, and other 14 molecules that are closely related to the discovered binders **1-6** but were not present in the library used for docking. A total of 16 of the ordered compounds belong to the thiobarbiturate chemotype, which was considered very promising from the previous results. Ten of the 28 compounds (ligands **7-16**) showed an IC<sub>50</sub> < 100 μM. Among the thiobarbiturate derivatives **7-10**, ligand **8** is the most potent (IC<sub>50</sub> = 6 μM, LE = 0.36). The carboxylic acid substituent is likely to contribute to the binding affinity, as the solvent-exposed portion of the DF2 binding pocket is rich in positively charged residues (K490, K416, and R527), which typically interact with the negatively charged phosphates of RNA, its natural substrate. Other molecules closely related to the thiobarbiturates were identified as interesting binders: the barbiturates **11** and **12**, the triazine **13**, and the condensed bicycles **14-16**. The X-ray crystal structures of compounds **13** and **15** confirm their binding (Figure 2f-g), showing again the sulfur atom interacting within the lipophilic tryptophan cage. Compound **15** can establish all of the interactions

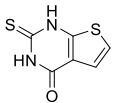
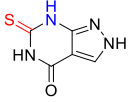
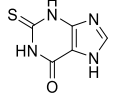
previously discussed: in addition to the interactions of m<sup>6</sup>-adenine, it can interact with both D422 and D528. Unfortunately, this doesn't translate into a very strong binding (IC<sub>50</sub> = 84 μM). This might be because the major tautomer represented in Table 1 is in equilibrium with other tautomeric forms which are not ideal for efficient binding (~ 67 % of desired tautomer, as calculated with the Chemaxon tautomers generator plugin <https://plugins.calculators.cxn.io/tautomers/>). Compounds **13** and **14** are characterized by a very favorable ligand efficiency of 0.73 and 0.60, respectively. We decided to further explore the derivatization of compound **14** because of its favorable ligand efficiency, the two possible vectors for substitution at two carbon atoms of its thiophene ring, respectively, and the relatively accessible synthesis (see below).



**Figure 2.** Crystal structures of DF2/fragment complexes. (a-g) Binding modes of m<sup>6</sup>-Adenine (compound **1** in Ref.<sup>13</sup>, PDB: 7YWB), compounds **3** (PDB: 9QEM), **4** (PDB: 9QEL), **5** (PDB: 9QEO), **6** (PDB: 9QFI), **13** (PDB: 9QIU) and **15** (PDB: 9QFL), respectively. The conserved water molecule (red sphere) and the hydrogen bonds (yellow dashed lines) are also shown. (h) Structural overlap of panels a-g. The carbon atoms of the ligands are in green and those of the protein in cyan.

**Table 1. m<sup>6</sup>-adenine and 16 ligands of DF2 identified by docking followed by SAR by catalogue.**

Compound nr.	2D structure <sup>a</sup>	Residual signal at 1 mM concentration (%) <sup>b</sup>	IC <sub>50</sub> [μM] <sup>c</sup> (LE <sup>d</sup> )	PDB code (Resolution [Å])
<b>m<sup>6</sup>-Adenine</b>		75 (Ref. <sup>13</sup> )	-	7YWB (1.92)
<b>1</b>		26	19 (0.50)	
<b>2</b>		12	172 (0.29)	
<b>3</b>		NA*	52 % at 125 μM #	9QEM (2.26)
<b>4</b>		18	246 (0.49)	9QEL (1.86)
<b>5</b>		88	-	9QEO (1.98)
<b>6</b>		80	-	9QFI (1.91)
<b>7</b>		NA*	21 (0.34)	
<b>8</b>		5	6 (0.36)	
<b>9</b>		NA*	30 (0.34)	
<b>10</b>		48	28 (0.33)	
<b>11</b>		30	29 (0.48)	
<b>12</b>		NA*	40 (0.32)	
<b>13</b>		5	52 (0.73)	9QIU (2.46)

<b>14</b>		NA*	16 (0.60)	
<b>15</b>		17	84 (0.51)	9QFL (1.70)
<b>16</b>		2	29 (0.57)	

Compounds **1-6** were identified by docking while compounds **7-16** were selected by SAR by catalogue. <sup>a</sup> The NH group interacting as hydrogen bond donor with the backbone carbonyl of C433 (blue) and the group in the bottom of the tryptophan-cage (red) are emphasized for the compounds with crystal structure in the complex with DF2. <sup>b</sup> The residual signal (with respect to DMSO control) at 1 mM compound concentration is measured using an HTRF-based binding assay as previously reported.<sup>26</sup> The signal decreases (with respect to buffer-only measurement) when the fragment competes with the binding of the natural ligand, i.e., m<sup>6</sup>A-oligoRNA. Thus, the lower the signal, the higher the affinity of the fragment. The reported values are the average of two technical replicates. <sup>c</sup> The IC<sub>50</sub> value for the DF2 reader domain was measured only for the fragments that, at a concentration of 1 mM, decrease the signal by more than 60%. <sup>d</sup> Ligand efficiency calculated according to  $LE = -\frac{\Delta G}{n_{HA}} \approx -RT \frac{\ln IC_{50}}{n_{HA}}$ . \* Interference or poor solubility observed at 1 mM. # Interference or poor solubility observed at higher concentrations, IC<sub>50</sub> could not be determined.

### Derivatization of compound **14**

The exploration of analogues of **14** has been pursued by synthesizing new derivatives (Table 2, S4) and ordering commercially available variants (Table S3). The replacement of the exocyclic sulfur atom with oxygen was detrimental for the potency, from 16 to 292 μM (compound **S61**). Several 5- and 6-membered ring alternatives to the thiophene were explored (compounds **15**, **16**, **S5**, **S62-64**), and only compound **16** resulted in an IC<sub>50</sub> comparable to the one of fragment **14** (29 μM vs 16 μM).

The medicinal chemistry campaign focused on derivatizing the thiophene ring of **14** through the addition of R<sup>1</sup> and/or R<sup>2</sup> groups (Table 2, Table S4). A total of 32 molecules were synthesized (Table S4). Table 2 shows the molecules with higher affinity than compound **14** as measured by the HTRF-based binding assay and/or a fluorescent polarization (FP). We were not able to solve the crystal structure of **14** in complex with DF2. Thus we hypothesized a similar binding mode as in the crystal structure with compound **15** (Figure 3a). The putative binding poses will be further analyzed and discussed in the next section.

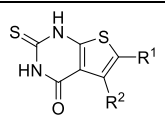
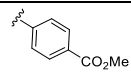
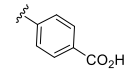
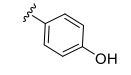
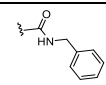
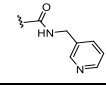
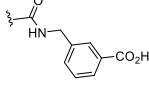
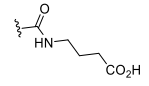
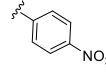
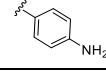
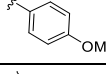
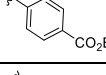
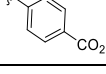
Compound **S74** (R<sup>2</sup> = Phenyl) and its derivatives (**17-19**, **S75-76**) were synthesized to try to obtain a favorable π-π stacking interaction with Y418, as seen in the X-ray crystal structure of the N-Methyl-3-phenyl-1H-pyrazolo[4,3-d]pyrimidin-7-amine (compound **7** in Ref.<sup>13</sup>, PDB: 7YXE). Among these compounds, **17** and **18** resulted in a 3-fold improved IC<sub>50</sub> in HTRF-based binding assay (Table 2), possibly due to a hydrogen bond between the carbonyl group and the hydroxyl of Y418 or the -NH<sub>2</sub> of N462. At R<sup>1</sup> we started with small polar substituents to try to establish interactions with D528 and/or with the structural water molecule or to try to replace the water molecule (compounds **20**, **21**, **S79-80**).

**Table 2. Expansion of hit fragment **14**.**

The ethyl ester of **21** at R<sup>1</sup> enhanced the binding (IC<sub>50</sub> = 6 μM), as also the bulkier benzyl (**22**, IC<sub>50</sub> = 10 μM) and methylpyridine (**23**, IC<sub>50</sub> = 10 μM) groups, both connected to the thiophene via an amide bond. We hypothesized that the -CH<sub>2</sub>- linker enables the aromatic ring to orient toward the solvent exposed region of the pocket, which is enriched with positively charged residues that facilitate binding to the negatively charged RNA. Based on this, we explored modifications such as adding a carboxylic acid (**24**) and further increasing the flexibility by replacing the benzyl group with an alkyl chain (**25**, **S83**). However, none of these changes led to an improvement in potency.

We continued the exploration of R<sup>1</sup> with substituted benzyl and phenyl rings directly connected to the thiophene (compounds **26-30**, **S84-87**). Compounds **26** and **27** resulted in an improvement of three- to fourfold compared to fragment **14**.

An FP competition assay was used to further validate the binding of the compounds to DF2. The main difference with respect to a previously published FP assay<sup>30</sup> is the use of an oligo-DNA as competitor ligand (see Material and Methods section). For most compounds, there is a factor of 2 to 5 difference between the IC<sub>50</sub> values for DF2 measured by HTRF and FP (Table 2). The largest discrepancy is a factor of 16 for compound **19** (32 μM and 2 μM by HTRF and FP, respectively). These differences might originate from the varying conditions in the two assays, such as the competitor mRNA (5'- Biotin-AAGAACCGG(m6A)CUAAGCU-3') in FRET and DNA (5'-FAM-AAGAACCGG(m6A)CTAAGCT-3') in FP, the salt concentration (150 mM NaCl and 100 mM KF in FRET, and 150 mM NaCl in FP), and the pH (7.5 in FRET and 7.4 in FP). The FP-based assay was also employed to assess the selectivity against DC1 and DC2 (see Selectivity section).

						
Compound nr.	R <sup>1</sup>	R <sup>2</sup>	HTRF assay IC <sub>50</sub> YTHDF2 [μM] <sup>a</sup> (LE <sup>b</sup> )	FP assay IC <sub>50</sub> YTHDF2 [μM] <sup>c</sup>	FP assay IC <sub>50</sub> YTHDC2 [μM] <sup>c</sup>	FP assay IC <sub>50</sub> YTHDC1 [μM] <sup>c</sup>
14	H	H	16 (0.60)	6	125	51
17	H		5 (0.35)	2	9	8
18	H		5 (0.36)	1	11	11
19	H		32	2	57	43
20	COCH <sub>3</sub>	CH <sub>3</sub>	13	5	66	75
21	CO <sub>2</sub> Et	CH <sub>3</sub>	6 (0.42)	7	335	57
22		CH <sub>3</sub>	10 (0.31)	16	387	147
23		CH <sub>3</sub>	10 (0.31)	2	646	188
24		CH <sub>3</sub>	20	4	58	38
25		CH <sub>3</sub>	14	2	185	51
26		CH <sub>3</sub>	6 (0.34)	27	50	97
27		CH <sub>3</sub>	4 (0.39)	3	43	22
28		H	22	3	13	15
29		H	21	5	12	8
30		H	16	3	7	12
31	H	CONH <sub>2</sub>	14 (0.47)	3	26	64

Compounds **17-31** are more active for DF2 than compound **14** in the HTRF and/or the FP assays. <sup>a</sup> The reported values for compounds **14, 18, 21, 23, 26, 27, 31** were measured by two or three biological replicates and for compounds **17, 19, 20, 22, 24, 25, 28-30** by a single biological replicate. Each biological replicate is the average of two technical replicates. The dose-response curves can be found in Figure S1; <sup>b</sup> The ligand efficiency calculated according to  $LE = -\frac{\Delta G}{n_{HA}} \approx -RT \frac{\ln IC_{50}}{n_{HA}}$  is shown for the fragment **14** and

its derivatives with HTRF  $IC_{50} \leq 10 \mu M$ ; <sup>c</sup>The reported values come from the average of the  $IC_{50}$ s of one (DC1) or two (DF2 and DC2) biological replicates, each replicate is the average of four technical replicates. The dose-response curves can be found in Figures S2 (DF2), S3 (DC2), S4 (DC1).

## Computational analysis

We could not determine the crystal structure of the complex of DF2 with compound **14** or any of its derivatives by soaking the ligands into apo DF2 crystals or co-crystallization. Thus, we employed MD simulations to investigate the binding mode of **14**, and its two derivatives **17** and **27** (Figure 3). As already observed during the docking campaign, the symmetry of the thiourea substructure is congruent with two distinct poses (A and B) which are flipped by a rotation of 180 degrees around the S=C double bond. For each compound and pose, eight independent 0.2- $\mu s$  MD simulations were performed for a cumulative sampling of 3.2  $\mu s$  per compound, starting from the docked poses of compound **14**, or the alignment of the derivatives **17** and **27** to it.

The analysis of the MD trajectories was carried out by adapting the protocol described in Ref.<sup>31</sup> (see Methods). Only the second half of each MD run, i.e., the trajectory segments from 100 ns to 200 ns, was used for the analysis to allow for sufficient ligand relaxation. From these segments we extracted the simulation frames where the compound is bound, defined as having a distance lower than 5 Å between the exocyclic sulfur atom and the N atom of C433 (Figure 3d). The percentage of bound frames are 94% and 77% for compound **14** in poses A and B, respectively; 57% and 89% for compound **17**; 85% and 74% for compound **27**. We calculated a set of 10 distances between the heavy atoms of the compounds (all located in the scaffold, i.e. present in compound **14**) and the binding pocket. Then, Principal Component Analysis (PCA) was used to project the multi-dimensional space into two dimensions. The two-dimensional data were then clustered using the Gaussian Mixture algorithm. The trajectory frame closest to the center of each cluster (centroid) was extracted and used as reference pose (Figure 3e).

Figure 3a shows the two reference poses obtained for compound **14** compared to the crystal structure of compound **15**. In both poses, the exocyclic sulfur atom is positioned within the lipophilic tryptophan cage. As mentioned above, compound **14** can adopt two distinct orientations which are related by a 180-degree rotation. This flipping rearranges the hydrogen bond interactions while preserving the same number of favorable polar contacts. In both poses, the two NH groups of the thiourea act as hydrogen bond donors for the backbone carbonyl of C433 and the side chain

of D422, respectively. Moreover, the carbonyl group and the thiophene sulfur atom are inverted between the two poses. In pose A, the carbonyl oxygen interacts with the backbone NH of Y418, as observed for the crystal structure with compound **15** (Figure 2g, 3a top). In pose B, it instead forms a hydrogen bond with the conserved water molecule (Figure 3a bottom). The sulfur atom in the thiophene ring points towards the structural water in pose A and the backbone NH of Y418 in pose B. In both poses, it acts as a weak hydrogen bond acceptor.<sup>32-34</sup> The root mean square deviation (RMSD) analysis of the MD runs started from the two poses suggests that pose A is slightly more stable (Figure 3d, top). The same is deduced from the distance between the exocyclic sulfur atom and C433.

A similar analysis was performed for compounds **17** and **27** to investigate the impact of bulky R<sup>1</sup> and/or R<sup>2</sup> substituents on the stability of the two poses. For compound **17** a smaller RMSD is observed for the B pose in comparison to A (Figure 3d). No such clear difference emerges for compound **27**. A similar pattern is observed when monitoring the distance between the exocyclic sulfur atom and C433. The most stable poses are shown in Figure 3b (compound **17**, pose B) and 3c (compound **27**, pose A).

## Selectivity

The HTRF-based assay was employed to evaluate the selectivity of the series against the other DF proteins. The compounds were tested at the concentration of 100  $\mu M$  and most of them inhibit also DF1 and DF3. (Table S5).

A dose-response experiment on DF1 and DF3 was conducted for compounds **17**, **18**, **23**, and **27** (Figure S5). Compounds **17**, **18**, and **27** are active on the three DF proteins. Their  $IC_{50}$  values for DF1 are approximately twice as high as for DF2, while for DF3, they are 4 to 12 times higher. In contrast, compound **23** is selective for DF2, with residual signals (at the highest employed concentration of 62.5  $\mu M$ ) of 51% and 87% for DF1 and DF3, respectively.

The binding affinity against DC1 could not be evaluated by HTRF because of interference of the compounds with the assay, which has a smaller assay window when performed with DC1 compared to the DF proteins. Thus, the FP assay was used to evaluate binding to DC1 and DC2. The affinity of the compounds for DC2 varied significantly depending on the substituents, with  $IC_{50}$  value ranging from 7  $\mu M$  for compound **30** to over 500  $\mu M$  for compounds **23**, **S74**, **S78**, **S79**, **S82**, **S83**, and **S89** (Tables 2 and S4).

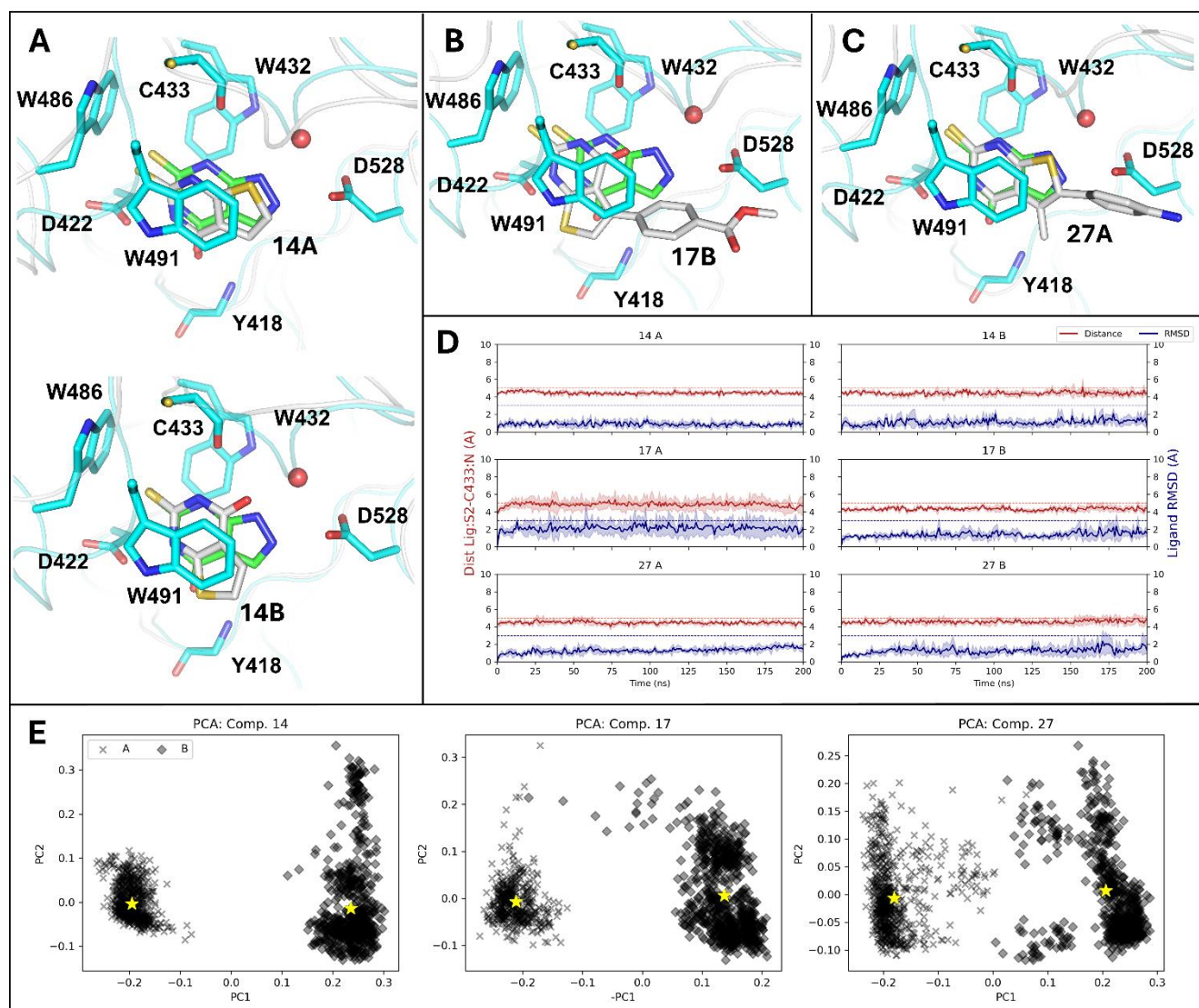


**Figure 3.** Predicted binding modes of compounds **14**, **17**, and **27** in DF2. (a) The pseudo-symmetry of fragment **14** (carbon atoms in gray) results in two binding modes called here A (a, top) and B (a, bottom). The crystal structure of DF2 (cyan) in complex with fragment **15** (carbon atoms in green, PDB: 9QFL) is overlapped for comparison. (b,c) Most populated pose of compounds **17** (pose B) and **27** (pose A). Their alternative poses are shown in Figure S6. (d) Analysis of the molecular dynamics simulations (MD) started from the two potential poses (pose A, left; pose B, right). The time series show the median distance between the exocyclic sulfur and the backbone N atom of C433 (red, with colored band representing one mean absolute deviation around the median, left y-axis). The ligand root mean square deviation (RMSD) with respect to the first frame is also shown (blue, right y-axis). (e) Principal Component Analysis (PCA) projections of the distances between atoms of the ligand and representative residues of the DF2 binding site. Data for MD snapshots saved every 1 ns are shown for the two poses (A, cross; B, diamond), and the centers of the two clusters are emphasized (yellow star).

The parent scaffold, compound **14**, exhibits approximately a 20-fold and 8-fold higher binding affinity for DF2 compared to DC2 and DC1 with  $IC_{50}$  values of 6  $\mu$ M, 125  $\mu$ M, and 51  $\mu$ M, respectively, as measured by FP (Table 2). Many derivatives maintain a strong preference for DF2. Notably, compound **23** shows high selectivity, being about 300 and 100 times more potent for DF2 than DC2 and DC1, respectively. In contrast, compounds with a substituted phenyl ring directly connected to the thiophene ( $R^1$  or  $R^2$ ) exhibited little to no selectivity against the DC proteins (e.g., ratio  $IC_{50}$  DC1/DF2 and DC2/DF2 of only 2-4 for ligands **29** and **30**).

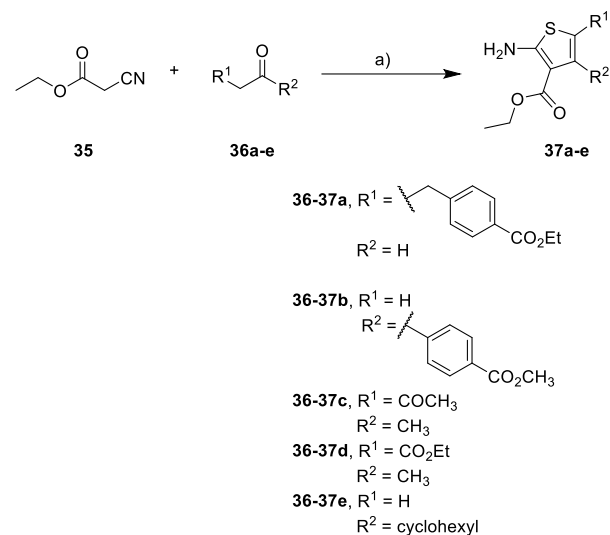
Compounds **17**, **18**, and **28-30** are the most potent DC binders of the series. They feature benzoic acid (at  $R^2$  in compound **18** and  $R^1$  in **30**), benzoic ester (at  $R^2$  in **17** and  $R^1$  in **29**), or para-methoxyphenyl (at  $R^1$  in **28**). Their similar behavior indicates that the previously discussed two poses (A and B, see previous section) may also be populated in the DC1 and DC2 binding sites. These results suggest that the substituent, whether at  $R^1$  or  $R^2$ , likely occupies the same region of the binding pocket. To the best of our knowledge, the only previously identified DC2-binder in the literature is the pan-YTH binder 'N-7', with a reported  $IC_{50}$  of 30  $\mu$ M

(as measured by FP).<sup>30</sup> Thus compounds **17** and **30** are the most potent DC2 ligands as of today (IC<sub>50</sub> values of 9 μM and 7 μM, respectively, measured by FP).

## Chemistry

The general synthetic approach begins with the synthesis of the ethyl 2-aminothiophene-3-carboxylate derivatives (**37a-g**), with the corresponding R<sup>1</sup> and/or R<sup>2</sup> substituents. For compounds **37a-e** this was achieved via a classic one-pot Gewald reaction (Scheme 1).<sup>35,36</sup>

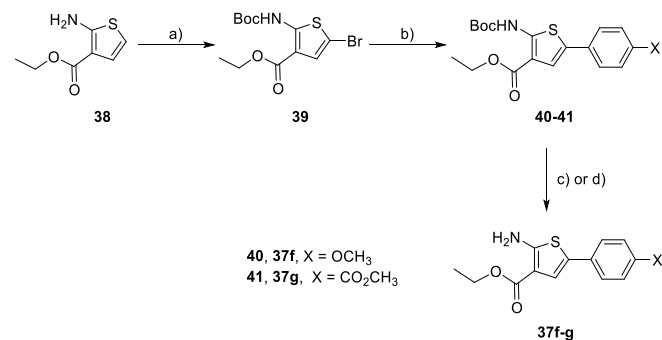
### Scheme 1. Synthesis Route for compounds 37a-e<sup>a</sup>



<sup>a</sup>Reagents and conditions: (a) for **37a-d**: S<sub>8</sub>, morpholine, EtOH, 70 °C; for **37e**: S<sub>8</sub>, morpholine, rt.

For the preparation of compounds **37g-m**, the substituted phenyl group was added via a Suzuki-Miyaura coupling from compound **39** (Scheme 2), prepared by bromination and protection of compound **38**.<sup>37,38</sup> Finally, the amino group was deprotected affording ethyl 2-aminothiophene-3-carboxylate intermediates **35g-i**.

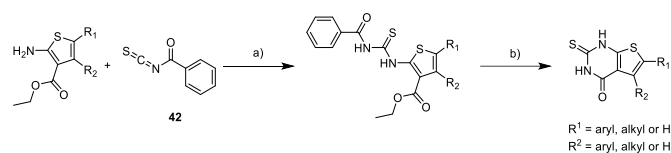
### Scheme 2. Synthesis Route for compounds 37f-g<sup>a</sup>



<sup>a</sup>Reagents and conditions: (a) (i) Boc<sub>2</sub>O, DMAP, dioxane, 0 to 80 °C; (ii) NBS, AcOH/DCM, -15 °C (b) Boronic acid, K<sub>2</sub>PO<sub>3</sub>, Pd(PPh<sub>3</sub>)<sub>4</sub>, DMF/H<sub>2</sub>O, 80 °C; (c) TFA, DCM; (d) HCl 4N in dioxane, MeOH.

Finally, the synthesized 2-aminothiophene-3-carboxylate intermediates (**37a-g**), and the commercially available ones (see SI), were reacted with benzoyl isothiocyanate **42** (Scheme 3). The ring closure was then performed in basic conditions under reflux.<sup>39</sup> The synthesis of some final compounds required additional transformations, including hydrolysis (**18, 24, 25, 30, S80, S87**), reduction (**27, S79**), and amide coupling (**22-25, S81-83**). Full experimental details are provided in the Supporting Information.

### Scheme 3. Synthesis Route for the bicyclic final compounds<sup>a</sup>



<sup>a</sup>Reagents and conditions: (a) CH<sub>3</sub>CN, 45 °C; (b) EtONa, EtOH, reflux.

## Conclusions

We have employed a fragment-based approach for identifying ligand-efficient small molecules that occupy the m<sup>6</sup>A-RNA recognition pocket of the DF2 reader domain. A crystal structure and molecular dynamics snapshot were used for high-throughput fragment docking. Each of the two docking campaigns yielded three active compounds and thus an overall hit rate of 13% (6/47). SAR by catalogue and the synthesis of 32 derivatives of the thio-thienopyrimidinone scaffold resulted in a series of ligand-efficient low-micromolar binders of DF2. Most members of the series are selective against DC1 and DC2, while they bind with low-micromolar affinity also to DF1 and DF3. In contrast, compound **23** displays distinct selectivity as it binds exclusively to DF2 (IC<sub>50</sub> of 2 μM and 10 μM measured by FP and HTRF, respectively). Finally, a few compounds (e.g., **17** and **18**) bind similarly to the five YTH-containing proteins. Among them, compounds **17** and **30** are currently the most potent ligands of DC2 (IC<sub>50</sub> values of 9 μM and 7 μM, respectively, measured by FP). We have also presented the crystal structures of DF2 in complex with six ligands which represent six distinct chemotypes (compounds **3-6, 13, and 15**). This structural data is useful for the development of new series of ligands of the YTHDF m<sup>6</sup>A-RNA readers, and for the further training of machine learning models.<sup>40</sup>

## Materials and methods

### Fragment docking and ranking

We used high-throughput docking to identify small-molecule binders of the m<sup>6</sup>A reader YTHDF2. The structure of the YTHDF2 domain used for docking is the one in the complex with the ligand 6-cyclopropyl-1H-pyrimidine-2,4-dione (PDB code: 7R5W)<sup>13</sup>. We prepared the protein structure for docking using CAMPARIv5.<sup>41</sup> The SEED<sup>21,22,42</sup> docking

program was used for rigid docking to the crystal structure itself and a snapshot obtained by MD simulations. These MD simulations were described in a previous study.<sup>13</sup> After clustering the snapshots, a representative pose with a large aperture of the m<sup>6</sup>A binding site was selected (volume of 600 Å<sup>3</sup> vs 324 Å<sup>3</sup> in the crystal structure). The pocket volume was obtained by structural alignment of the crystal structure (PDB 7R5W) and the MD snapshot, and using the dpocket functionality of the fpocket tool with the ligand as reference.<sup>43</sup> A library of 500,000 small molecules was considered for screening by SEED. The molecules were selected from the ZINC2020 database<sup>23</sup> with the number of non-hydrogen atoms between 11 and 20, at least one ring and one sp<sup>3</sup> carbon in the structure. For each of the extracted compounds, up to 20 conformers were generated using a distance geometry-based algorithm.<sup>24</sup>

The two protein structures were kept rigid during docking and evaluation of the binding energy. The binding site definition for SEED docking consisted of the single residue C433. A structural water molecule was conserved as part of the active site because it is consistently resolved in all the crystal structures obtained and is involved as a hydrogen bond acceptor and donor with the side chains of W432 and D528, respectively.<sup>13,25</sup> The partial charges and van der Waals parameters for the atoms in the protein and the small molecules were taken from the CHARMM36 all-atom force field<sup>44–46</sup> and the CHARMM general force field (CGenFF),<sup>47</sup> respectively. Importantly, the CHARMM36 force field and CGenFF are fully consistent in their partial charges and van der Waals parameters. The evaluation of the binding energy in the program SEED consists of a force field-based energy function with a continuum dielectric approximation of desolvation penalties by the generalized Born model.<sup>48</sup> The values of the dielectric constant were 2.0 and 78.5 for the regions of space occupied by the solute and solvent, respectively. Fragment screening by SEED requires about 1 s per fragment. SEED is available as an open-source code from GitLab (<https://gitlab.com/CaflischLab>).

From both docking campaigns, the compounds were ranked according to two energy terms calculated by SEED, namely the total binding energy (SEED total), and the difference between the electrostatic contribution to the intermolecular interaction energy in the solvent and the solvation energy of the ligand (Delec). The top scoring compounds were then selected if they showed the crucial hydrogen bond with the backbone carbonyl of C433 and at least one other interaction within the active site. Finally, 47 compounds were purchased on the basis of commercial availability and structural diversity: 25 selected from the docking performed on the crystal structure and 22 from that on the MD snapshot with large aperture of the binding site.

### HTRF Assay

GST-YTHDC1, GST-YTHDF1, GST-YTHDF2, and GST-YTHDF3 were purified as previously reported.<sup>26</sup> The HTRF assay was assembled as detailed in Ref.<sup>13</sup> with the only difference being that the starting concentration of the dose-response experiments used for the IC<sub>50</sub> determination was

varied dependently from the tested compound. The same protocol applies to the four proteins. The competitive inhibition data of GST-YTHDF1 (single dose experiment at 100 μM compound concentration and dose-response curves), GST-YTHDF3 (single dose experiment at 100 μM compound concentration and dose-response curves), and GST-YTHDF2 (single dose experiment at 100 μM compound concentration) were normalized as described in Ref.<sup>27</sup> to mitigate interference. The signal was measured as described in Ref.<sup>27</sup>

### GST-YTHDC2 production

The N-terminally GST-tagged YTH domain of YTHDC2 (residues 1285–1424, cloned into the pGEX-6P-1 vector) was overexpressed in Rosetta (DE3) cells overnight at 20 °C following induction with 0.4 mM IPTG. The cells were harvested and resuspended in lysis buffer containing 100 mM Tris-HCl (pH 8.0) and 500 mM NaCl. After cell lysis, the lysate was clarified by centrifugation at 48,000 g for one hour, and the soluble proteins were loaded onto a column packed with Glutathione Sepharose 4B (GE Healthcare), then eluted with 20 mM reduced glutathione in lysis buffer. Finally, a size-exclusion chromatography step (HiLoad 16/600 Superdex 200 pg column, GE Healthcare) was performed to further purify the protein in 20 mM Tris-HCl (pH 7.4) and 150 mM NaCl.

### DNA-Fluorescence polarization (FP) assay

For fluorescence polarization (FP) experiments, a 5'-fluorescein-labeled m<sup>6</sup>A-DNA probe (5'-FAM-AAGAACCGG(m<sup>6</sup>A)CTAAGCT-3') was synthesized by Microsynth AG.

The final concentration of the fluorescein-labeled DNA was kept constant at 3 nM. For YTHDC2 measurements, the protein concentration was set to 25 nM, while for YTHDF2 measurements, it was set to 10 nM, and for YTHDC1 it was set at 15 nM. The compound concentration was serially diluted to obtain the dose-response curve. The competition experiments were conducted in a final volume of 20 μL in a buffer containing 20 mM Tris-HCl (pH 7.4), 150 mM NaCl, and 0.01% BSA, using a 384-well black flat-bottom microplate (Corning 3575).

After incubating the mixture for 1 hour, the anisotropy values were measured using a Tecan SPARK plate reader with 485/20 nm excitation and 535/25 nm emission polarization filters, suitable for fluorescein, at 25 °C. The IC<sub>50</sub> values were derived by fitting a dose-response curve to the data using non-linear regression analysis in GraphPad Prism.

### YTHDF2 Protein crystallography and soaking

The YTH domain of YTHDF2 was expressed, purified, crystallized and soaked as described in Ref.<sup>13</sup> The X-ray diffraction experiment was performed on the X06DA beamline of Paul Scherrer institute's Swiss Light Source. Resulting data were analyzed as described in Ref.<sup>13</sup>

## Molecular dynamics simulations and clustering

We used molecular dynamics (MD) simulations to analyze the interactions between the YTHDF2 domain and compounds **14**, **17** and **27**. Compound **14** (and its derivatives **17** and **27**) can in principle bind in two poses due to the symmetry of its thiourea ring. This was also observed in the docking results of compound **14**. Therefore, we defined two poses, A and B, depending respectively on the orientation of the exocyclic sulfur atom pointing towards the tryptophan cage or outwards. We used the ParaLig<sup>49</sup> software to modify the two docked poses of compound **14** to obtain derivatives **17** and **27**. The protein/ligand structures were then prepared using the software CAMPARIv5.<sup>41</sup> Simulations were run using TIP3P (CHARMM) water model,<sup>50</sup> with a 0.15 M concentration of Na<sup>+</sup> and Cl<sup>-</sup> ions. We equilibrated the systems first using an NPT ensemble to reach 300 K and 1 bar, under 10 kJ/(mol Å<sup>2</sup>) positional restraints. We then applied four successive 1 ns NVT equilibrations with weakening restraints of 10, 5, 2.5, and 1.25 kJ/(mol Å<sup>2</sup>), respectively. All simulations were done using the CHARMM36m forcefield<sup>51</sup> with the July 2022 GROMACS port. Production MD simulations consisted of eight independent runs for each compound and pose, and a sampling of 200 ns per run. Production simulations were performed at the Swiss Supercomputing Center (CSCS) with the support of grant s1272 using GROMACS 2021.5.<sup>52</sup>

For clustering we first subsampled the trajectories by selecting MD frames at every nanosecond of the simulation segments from 100 ns to 200 ns. In other words, we discarded the first half of each run for allowing the ligand to equilibrate in the binding pocket. The bound frames were selected according to the distance between the N atom of C433 and the thiourea sulfur atom, and choosing frames with a distance lower than 5 Å. We applied PCA on a set of 10 protein-ligand distances to reduce the data to two dimensions. These 10 distances involved atoms of the thiourea ring and the residues C433 (four distances), D422 (two distances), Y418, W432, W486, W491 (one distance each). The Gaussian mixture algorithm with full covariance was employed for clustering the two-dimensional data on the PC space. The MD snapshot closest to the cluster centroid was used as representative poses. Analyses were done using MDTraj<sup>53</sup> and SciKit learn.<sup>54</sup>

## ASSOCIATED CONTENT

### Supporting Information.

The Supporting Information is available free of charge at <http://pubs.acs.org>.

Supplementary figures, tables, materials, synthetic procedures, characterization data, <sup>1</sup>H and <sup>13</sup>C NMR spectra, and HPLC traces for all final compounds (PDF).

X-ray data collection and refinement statistics for the 6 complex YTH-YTHDF2 crystal structures (XLSX).

### Accession Codes

9QEM (3), 9QEL (4), 9QEO (5), 9QFI (6), 9QIU (13), 9QFL (15). UniProt accession IDs: YTHDF1: Q9BYJ9; YTHDF2: Q9Y5A9; YTHDF3: Q7Z739; YTHDC1: Q96MU7; YTHDC2: Q9H6S0.

## AUTHOR INFORMATION

### Corresponding Author

\* **Amedeo Caffisch** – Department of Biochemistry, University of Zurich, CH-8057 Zurich, Switzerland; [orcid.org/0000-0002-2317-6792](https://orcid.org/0000-0002-2317-6792); Phone: +41 44 635 55 21; Email: [caffisch@bioc.uzh.ch](mailto:caffisch@bioc.uzh.ch)

### Authors

**Annalisa Invernizzi** - Department of Biochemistry, University of Zurich, Winterthurerstrasse 190, CH-8057, Zurich, Switzerland; [orcid.org/0009-0000-3380-8602](https://orcid.org/0009-0000-3380-8602)

**Francesco Nai** - Department of Biochemistry, University of Zurich, Winterthurerstrasse 190, CH-8057, Zurich, Switzerland; [orcid.org/0000-0002-4258-3174](https://orcid.org/0000-0002-4258-3174)

**Rajiv Kumar Bedi** - Department of Biochemistry, University of Zurich, Winterthurerstrasse 190, CH-8057, Zurich, Switzerland; [orcid.org/0000-0002-8193-9006](https://orcid.org/0000-0002-8193-9006)

**Pablo Andrés Vargas-Rosales** - Department of Biochemistry, University of Zurich, Winterthurerstrasse 190, CH-8057, Zurich, Switzerland; [orcid.org/0000-0001-5198-620X](https://orcid.org/0000-0001-5198-620X)

**Yaozong Li** - Department of Biochemistry, University of Zurich, Winterthurerstrasse 190, CH-8057, Zurich, Switzerland; [orcid.org/0000-0002-5796-2644](https://orcid.org/0000-0002-5796-2644)

**Elena Bochenkova** - Department of Biochemistry, University of Zurich, Winterthurerstrasse 190, CH-8057, Zurich, Switzerland;

**Marcin Herok** - Department of Biochemistry, University of Zurich, Winterthurerstrasse 190, CH-8057, Zurich, Switzerland; [orcid.org/0000-0003-0294-4040](https://orcid.org/0000-0003-0294-4040)

**František Zálešák** - Department of Biochemistry, University of Zurich, Winterthurerstrasse 190, CH-8057, Zurich, Switzerland.

### Notes

The authors declare no competing financial interest.

## ACKNOWLEDGMENT

The authors thank Beat Blattmann and Görkem Kurtuldu at the Protein Crystallization Center of UZH for the assistance with the crystallization, and the beamline scientists at the Swiss Light Source at Paul Scherrer Institute for their help with the X-ray diffraction experiments. We thank Maria Paula Flores Espinoza and Thomas Frei for their technical assistance. This work was financially supported by the Swiss National Science Foundation to A.C. (Grant number 310030\_212195), the Swiss Cancer Research Foundation to A.C. (Grant number KFS 5748-02-2023), the Swiss National Supercomputing Center (CSCS, project ID s1272 on Piz Daint), and the UZH Candoc Grant to A.I. (Grant number FK-24-031).

## ABBREVIATIONS

YTHDF, YT521-B homology domain family; m<sup>6</sup>A, N<sup>6</sup>-methyladenosine; YTHDC, YTH domain containing; oligoRNA, oligoribonucleotide; HTRF, homogeneous time-resolved fluorescence; LE, ligand efficiency; FP, fluorescence polarization; PCA, principal component analysis; RMSD, root mean square deviation.

## REFERENCES

- (1) Shi, H.; Wei, J.; He, C. Where, When, and How: Context-Dependent Functions of RNA Methylation Writers, Readers, and Erasers. *Mol. Cell* **2019**, *74* (4), 640–650. DOI: 10.1016/j.molcel.2019.04.025.
- (2) Liao, J.; Wei, Y.; Liang, J.; Wen, J.; Chen, X.; Zhang, B.; Chu, L. Insight into the Structure, Physiological Function, and Role in Cancer of M6A Readers—YTH Domain-Containing Proteins. *Cell Death Discov.* **2022**, *8* (137). DOI: 10.1038/s41420-022-00947-0.
- (3) Chen, L.; Gao, Y.; Xu, S.; Yuan, J.; Wang, M.; Li, T.; Gong, J. N6-Methyladenosine Reader YTHDF Family in Biological Processes: Structures, Roles, and Mechanisms. *Front. Immunol.* **2023**, *14*, 1162607. DOI: 10.3389/fimmu.2023.1162607.
- (4) Dai, X. Y.; Shi, L.; Li, Z.; Yang, H. Y.; Wei, J. F.; Ding, Q. Main N6-Methyladenosine Readers: YTH Family Proteins in Cancers. *Front. Oncol.* **2021**, *11*, 635329. DOI: 10.3389/fonc.2021.635329.
- (5) Xiao, W.; Adhikari, S.; Dahal, U.; Chen, Y. S.; Hao, Y. J.; Sun, B. F.; Sun, H. Y.; Li, A.; Ping, X. L.; Lai, W. Y.; Wang, X.; Ma, H. L.; Huang, C. M.; Yang, Y.; Huang, N.; Jiang, G. Bin; Wang, H. L.; Zhou, Q.; Wang, X. J.; Zhao, Y. L.; Yang, Y. G. Nuclear M6A Reader YTHDC1 Regulates mRNA Splicing. *Mol. Cell* **2016**, *61* (4), 507–519. DOI: 10.1016/j.molcel.2016.01.012.
- (6) Hsu, P. J.; Zhu, Y.; Ma, H.; Guo, Y.; Shi, X.; Liu, Y.; Qi, M.; Lu, Z.; Shi, H.; Wang, J.; Cheng, Y.; Luo, G.; Dai, Q.; Liu, M.; Guo, X.; Sha, J.; Shen, B.; He, C. Ythdc2 Is an N6-Methyladenosine Binding Protein That Regulates Mammalian Spermatogenesis. *Cell Res.* **2017**, *27* (9), 1115–1127. DOI: 10.1038/cr.2017.99.
- (7) Kretschmer, J.; Rao, H.; Hackert, P.; Sloan, K. E.; Höbartner, C.; Bohnsack, M. T. The M6A Reader Protein YTHDC2 Interacts with the Small Ribosomal Subunit and the 5′–3′ Exoribonuclease XRN1. *RNA* **2018**, *24* (10), 1339–1350. DOI: 10.1261/rna.064238.117.
- (8) Lasman, L.; Krupalnik, V.; Viukov, S.; Mor, N.; Aguilera-Castrejon, A.; Schneir, D.; Bayerl, J.; Mizrahi, O.; Peles, S.; Tawil, S.; Sathe, S.; Nachshon, A.; Shani, T.; Zerbib, M.; Kilimnik, I.; Aigner, S.; Shankar, A.; Mueller, J. R.; Schwartz, S.; Stern-Ginossar, N.; Yeo, G. W.; Geula, S.; Novershtern, N.; Hanna, J. H. Context-Dependent Functional Compensation between Ythdf M6A Reader Proteins. *Genes Dev.* **2020**, *34* (19–20), 1373–1391. DOI: 10.1101/gad.340695.120.
- (9) Li, F.; Zeng, C.; Liu, J.; Wang, L.; Yuan, X.; Yuan, L.; Xia, X.; Huang, W. The YTH Domain-Containing Protein Family: Emerging Players in Immunomodulation and Tumour Immunotherapy Targets. *Clin. Transl. Med.* **2024**, *14* (8), e1784. DOI: 10.1002/CTM2.1784.
- (10) Li, J.; Meng, S.; Xu, M.; Wang, S.; He, L.; Xu, X.; Wang, X.; Xie, L.; Li, J.; Meng, S.; Xu, M.; Wang, S.; He, L.; Xu, X.; Wang, X.; Xie, L. Downregulation of N6-Methyladenosine Binding YTHDF2 Protein Mediated by MiR-493-3p Suppresses Prostate Cancer by Elevating N6-Methyladenosine Levels. *Oncotarget* **2017**, *9* (3), 3752–3764. DOI: 10.18632/oncotarget.23365.
- (11) Einstein, J. M.; Perelis, M.; Chaim, I. A.; Meena, J. K.; Nussbacher, J. K.; Tankka, A. T.; Yee, B. A.; Li, H.; Madrigal, A. A.; Neill, N. J.; Shankar, A.; Tyagi, S.; Westbrook, T. F.; Yeo, G. W. Inhibition of YTHDF2 Triggers Proteotoxic Cell Death in MYC-Driven Breast Cancer. *Mol. Cell* **2021**, *81* (15), 3048–3064.e9. DOI: 10.1016/j.molcel.2021.06.014.
- (12) Wang, J. yan; Lu, A. qing. The Biological Function of M6A Reader YTHDF2 and Its Role in Human Disease. *Cancer Cell Int.* **2021**, *21* (109). DOI: 10.1186/s12935-021-01807-0.
- (13) Nai, F.; Nachawati, R.; Zálešák, F.; Wang, X.; Li, Y.; Caflich, A. Fragment Ligands of the M6A-RNA Reader YTHDF2. *ACS Med. Chem. Lett.* **2022**, *13* (9), 1500–1509. DOI: 10.1021/acsmchemlett.2C00303.
- (14) Micaelli, M.; Dalle Vedove, A.; Cerofolini, L.; Vigna, J.; Sighel, D.; Zaccara, S.; Bonomo, I.; Poulentzas, G.; Rosatti, E. F.; Cazzanelli, G.; Alunno, L.; Belli, R.; Peroni, D.; Dassi, E.; Murakami, S.; Jaffrey, S. R.; Fragai, M.; Mancini, I.; Lolli, G.; Quattrone, A.; Provenzani, A. Small-Molecule Ebselen Binds to YTHDF Proteins Interfering with the Recognition of N6-Methyladenosine-Modified RNAs. *ACS Pharmacol. Transl. Sci.* **2022**, *5* (10), 872–891. DOI: 10.1021/acspsci.2c00008.
- (15) Madia, V. N.; Messori, A.; Saccoliti, F.; Tudino, V.; Leo, A. De; Vita, D. De; Bortolami, M.; Scipione, L.; Pindinello, I.; Costi, R.; Santo, R. Di. Tegaserod for the Treatment of Irritable Bowel Syndrome. *Antinflamm. Antiallergy Agents Med. Chem.* **2019**, *19* (4), 342–369. DOI: 10.2174/1871523018666190911121306.
- (16) Zou, Z.; Wei, J.; Chen, Y.; Jin, P.; Luo, C.; Kang, Y.; Shi, H.; Yang, F.; Shi, Z.; Chen, S.; Zhou, Y.; Sepich-Poore, C.; Zhuang, X.; Zhou, X.; Jiang, H.; Wen, Z.; He, C. FMRP Phosphorylation Modulates Neuronal Translation through YTHDF1. *Mol. Cell* **2023**, *83*, 4304–4317.e8. DOI: 10.1016/j.molcel.2023.10.028.
- (17) Feng, G.; Wu, Y.; Hu, Y.; Shuai, W.; Yang, X.; Li, Y.; Ouyang, L.; Wang, G. Small Molecule Inhibitors Targeting M6A Regulators. *J. Hematol. Oncol.* **2024**, *17* (30). DOI: 10.1186/s13045-024-01546-5.
- (18) Nai, F. Development of Chemical Probes for Epitranscriptomic Proteins, University of Zurich, Faculty of Science, Zurich, **2024**. DOI: DOI: 10.5167/uzh-264334.
- (19) Wang, L.; Dou, X.; Chen, S.; Yu, X.; Huang, X.; Zhang, L.; Chen, Y.; Wang, J.; Yang, K.; Bugno, J.; Pitroda, S.; Ding, X.; Piffko, A.; Si, W.; Chen, C.; Jiang, H.; Zhou, B.; Chmura, S. J.; Luo, C.; Liang, H. L.; He, C.; Weichselbaum, R. R. YTHDF2 Inhibition Potentiates Radiotherapy Antitumor Efficacy. *Cancer Cell* **2023**, *41* (7), 1294–1308.e8. DOI: 10.1016/j.ccell.2023.04.019.
- (20) Qiu, X.; Kemker, C.; Goebel, G. L.; Lampe, P.; Wallis, N.; Schiller, D.; Bigler, K.; Jiang, M.; Sievers, S.; Yeo, G. W.; Wu, P. Phenylpyrazoles as Inhibitors of the M6A RNA-Binding Protein YTHDF2. *JACS Au* **2025**. DOI: 10.1021/jacsau.4c00754.
- (21) Majeux, N.; Scarsi, M.; Apostolakis, J.; Ehrhardt, C.; Caflich, A. Exhaustive Docking of Molecular Fragments With Electrostatic Solvation. *PROTEINS: Struct., Funct., and Genet.* **1999**, *37*, 88–105. DOI: 10.1002/(SICI)1097-0134(19991001)37:1<88::AID-PROT9>3.0.CO;2-O.
- (22) Goossens, K.; Wroblewski, B.; Langini, C.; van Vlijmen, H.; Caflich, A.; de Winter, H. Assessment of the Fragment Docking Program SEED. *J. Chem. Inf. Model* **2020**, *60* (10), 4881–4893. DOI: 10.1021/acs.jcim.0c00556.
- (23) Irwin, J. J.; Tang, K. G.; Young, J.; Dandarchuluun, C.; Wong, B. R.; Khurelbaatar, M.; Moroz, Y. S.; Mayfield, J.; Sayle, R. A. ZINC20 - A Free Ultralarge-Scale Chemical Database for Ligand Discovery. *J. Chem. Inf. Model.* **2020**, *60* (12), 6065–6073. DOI: 10.1021/acs.jcim.0c00675.
- (24) Riniker, S.; Landrum, G. A. Better Informed Distance Geometry: Using What We Know to Improve Conformation Generation. *J. Chem. Inf. Model.* **2015**, *55* (12), 2562–2574. DOI: 10.1021/acs.jcim.5b00654.
- (25) Li, Y.; Bedi, R. K.; Moroz-Omori, E. V.; Caflich, A. Structural and Dynamic Insights into Redundant Function of YTHDF Proteins. *J. Chem. Inf. Model.* **2020**, *60* (12), 5932–5935. DOI: 10.1021/acs.jcim.0C01029.
- (26) Wiedmer, L.; Eberle, S. A.; Bedi, R. K.; Śledź, P.; Caflich, A. A Reader-Based Assay for M6A Writers and Erasers. *Anal. Chem.* **2019**, *91* (4), 3078–3084. DOI: 10.1021/acs.analchem.8b05500.
- (27) Zálešák, F.; Nai, F.; Herok, M.; Bochenkova, E.; Bedi, R. K.; Li, Y.; Errani, F.; Caflich, A. Structure-Based Design of a Potent and Selective YTHDC1 Ligand. *J. Med. Chem.* **2024**, *67* (11), 9516–9535. DOI: 10.1021/acs.jmedchem.4C00599.

- (28) Sinnokrot, M. O.; Valeev, E. F.; Sherrill, C. D. Estimates of the Ab Initio Limit for  $\pi$ - $\pi$  Interactions: The Benzene Dimer. *J. Am. Chem. Soc.* **2002**, *124* (36), 10887–10893. DOI: 10.1021/ja025896h.
- (29) Zhao, Y.; Li, J.; Gu, H.; Wei, D.; Xu, Y. chang; Fu, W.; Yu, Z. Conformational Preferences of  $\pi$ - $\pi$  Stacking Between Ligand and Protein, Analysis Derived from Crystal Structure Data Geometric Preference of  $\pi$ - $\pi$  Interaction. *Interdiscip. Sci.* **2015**, *7* (3), 211–220. DOI: 10.1007/s12539-015-0263-z.
- (30) Wang, C. H.; Zhou, H. Discovery of a New Inhibitor for YTH Domain-Containing M6A RNA Readers. *RSC Chem. Biol.* **2024**, *5* (9), 914–923. DOI: 10.1039/d4cb00105b.
- (31) Nai, F.; Flores Espinoza, M. P.; Invernizzi, A.; Vargas-Rosales, P. A.; Bobileva, O.; Herok, M.; Cafilisch, A. Small-Molecule Inhibitors of the M7G-RNA Writer METTL1. *ACS Bio and Med Chem Au* **2024**, *4*, 2, 100–110. DOI: 10.1021/acsbiochemau.3c00030.
- (32) Van Bergen, L. A. H.; Alonso, M.; Palló, A.; Nilsson, L.; De Proft, F.; Messens, J. Revisiting Sulfur H-Bonds in Proteins: The Example of Peroxiredoxin AhpE. *Sci. Rep.* **2016**, *6*, 30369. DOI: 10.1038/srep30369.
- (33) Gregoret, L. M.; Rader, S. D.; Fletterick, R. J.; Cohen, F. E. Hydrogen Bonds Involving Sulfur Atoms in Proteins. *Proteins* **1991**, *9* (2), 99–107. DOI: 10.1002/prot.340090204.
- (34) Rao Mundlapati, V.; Ghosh, S.; Bhattacharjee, A.; Tiwari, P.; Biswal, H. S. Critical Assessment of the Strength of Hydrogen Bonds between the Sulfur Atom of Methionine/Cysteine and Backbone Amides in Proteins. *J. Phys. Chem. Lett.* **2015**, *6* (8), 1385–1389. DOI: 10.1021/acs.jpcclett.5b00491.
- (35) Sabnis, R. W.; Rangnekar, D. W.; Sonawane, N. D. 2-Aminothiophenes by the Gewald Reaction. *J. Heterocycl. Chem.* **1999**, *36* (2), 333–345. DOI: 10.1002/jhet.5570360203.
- (36) El-Mekabaty, A. Chemistry of 2-Amino-3-Carboxythythiophene and Related Compounds. *Synth. Commun.* **2014**, *44* (1), 1–31. DOI: 10.1080/00397911.2013.821618.
- (37) Dong, Y.; Navarathne, D.; Bolduc, A.; McGregor, N.; Skene, W. G.  $\alpha$ , $\alpha'$ -N-Boc-Substituted Bi- and Terthiophenes: Fluorescent Precursors for Functional Materials. *J. Org. Chem.* **2012**, *77*, 12, 5429–5433. DOI: 10.1021/jo300687d.
- (38) Aurelio, L.; Figler, H.; Flynn, B. L.; Linden, J.; Scammells, P. J. 5-Substituted 2-Aminothiophenes as A1 Adenosine Receptor Allosteric Enhancers. *Bioorg. Med. Chem.* **2008**, *16* (3), 1319–1327. DOI: 10.1016/j.bmc.2007.10.065.
- (39) Wang, T.; Zheng, C. H.; Liu, S.; Chen, H. Z. Synthesis and Biological Activity of a Series of New Thieno[2,3-d]Pyrimidines. *Phosphorus Sulfur Silicon Relat. Elem.* **2010**, *185* (7), 1543–1549. DOI: 10.1080/10426500903127565.
- (40) Vargas-Rosales, P. A.; Cafilisch, A. The Physics-AI Dialogue in Drug Design. *RSC Med. Chem.* **2025**. DOI: 10.1039/d4md00869c.
- (41) Vitalis, A.; Pappu, R. V. Chapter 3 Methods for Monte Carlo Simulations of Biomacromolecules. *Annu. Rep. Comput. Chem.* **2009**, *5*, 49–76. DOI: 10.1016/s1574-1400(09)00503-9.
- (42) Majeux, N.; Scarsi, M.; Cafilisch, A. Efficient Electrostatic Solvation Model for Protein-Fragment Docking. *PROTEINS: Struct., Funct., Genet.* **2001**, *42*, 256–268. DOI: 10.1002/1097-0134(20010201)42:2<256::AID-PROT130>3.0.CO;2-4.
- (43) Le Guilloux, V.; Schmidtke, P.; Tuffery, P. Fpocket: An Open Source Platform for Ligand Pocket Detection. *BMC Bioinformatics* **2009**, *10* (1), 1–11. DOI: 10.1186/1471-2105-10-168.
- (44) MacKerell, A. D.; Bashford, D.; Bellott, M.; Dunbrack, R. L.; Evansck, J. D.; Field, M. J.; Fischer, S.; Gao, J.; Guo, H.; Ha, S.; Joseph-McCarthy, D.; Kuchnir, L.; Kuczera, K.; Lau, F. T. K.; Mattos, C.; Michnick, S.; Ngo, T.; Nguyen, D. T.; Prodhom, B.; Reiher, W. E.; Roux, B.; Schlenkrich, M.; Smith, J. C.; Stote, R.; Straub, J.; Watanabe, M.; Wiórkiewicz-Kuczera, J.; Yin, D.; Karplus, M. All-Atom Empirical Potential for Molecular Modeling and Dynamics Studies of Proteins. *J. Phys. Chem. B* **1998**, *102*, 18, 3586–3616. DOI: 10.1021/jp973084f.
- (45) MacKerell, A. D.; Feig, M.; Brooks, C. L. Improved Treatment of the Protein Backbone in Empirical Force Fields. *J. Am. Chem. Soc.* **2004**, *126*, 3, 698–699. DOI: 10.1021/ja036959e.
- (46) Best, R. B.; Zhu, X.; Shim, J.; Lopes, P. E. M.; Mittal, J.; Feig, M.; MacKerell, A. D. Optimization of the Additive CHARMM All-Atom Protein Force Field Targeting Improved Sampling of the Backbone  $\phi$ ,  $\psi$  and Side-Chain X1 and X2 Dihedral Angles. *J. Chem. Theory Comput.* **2012**, *8* (9), 3257–3273. DOI: 10.1021/ct300400x.
- (47) Vanommeslaeghe, K.; Hatcher, E.; Acharya, C.; Kundu, S.; Zhong, S.; Shim, J.; Darian, E.; Guvench, O.; Lopes, P.; Vorobyov, I.; MacKerell, A. D. CHARMM General Force Field: A Force Field for Drug-like Molecules Compatible with the CHARMM All-Atom Additive Biological Force Fields. *J. Comput. Chem.* **2010**, *31* (4), 671–690. DOI: 10.1002/jcc.21367.
- (48) Scarsi, M.; Apostolakis, J.; Cafilisch, A. Continuum Electrostatic Energies of Macromolecules in Aqueous Solutions. *J. Phys. Chem. A* **1997**, *101* (43), 8098–8106. DOI: 10.1021/jp9714227.
- (49) Vitalis, A.; Parker, D.; Radler, F.; Vargas-Rosales, P. A.; Zhang, Y.; Marchand, J.-R.; Cafilisch, A. Parallelized Tools for the Preparation and Curation of Large Libraries for Virtual Screening. *J. Comput. Chem.* **2025**, *46* (7), e70074. DOI: 10.1002/jcc.70074.
- (50) Boonstra, S.; Onck, P. R.; Van Der Giessen, E. CHARMM TIP3P Water Model Suppresses Peptide Folding by Solvating the Unfolded State. *J. Phys. Chem. B* **2016**, *120* (15), 3692–3698. DOI: 10.1021/acs.jpcc.6b01316.
- (51) Huang, J.; Rauscher, S.; Nawrocki, G.; Ran, T.; Feig, M.; De Groot, B. L.; Grubmüller, H.; MacKerell, A. D. CHARMM36m: An Improved Force Field for Folded and Intrinsically Disordered Proteins. *Nature Methods* **2016**, *14* (1), 71–73. DOI: 10.1038/nmeth.4067.
- (52) Abraham, M. J.; Murtola, T.; Schulz, R.; Páll, S.; Smith, J. C.; Hess, B.; Lindahl, E. GROMACS: High Performance Molecular Simulations through Multi-Level Parallelism from Laptops to Supercomputers. *SoftwareX* **2015**, *1–2*, 19–25. DOI: 10.1016/j.softx.2015.06.001.
- (53) McGibbon, R. T.; Beauchamp, K. A.; Harrigan, M. P.; Klein, C.; Swails, J. M.; Hernández, C. X.; Schwantes, C. R.; Wang, L. P.; Lane, T. J.; Pande, V. S. MDTraj: A Modern Open Library for the Analysis of Molecular Dynamics Trajectories. *Biophys. J.* **2015**, *109* (8), 1528–1532. DOI: 10.1016/j.bpj.2015.08.015.
- (54) Pedregosa, F.; Varoquaux, G.; Gramfort, A.; Michel, V.; Thirion, B.; Grisel, O.; Blondel, M.; Prettenhofer, P.; Weiss, R.; Dubourg, V.; Vanderplas, J.; Passos, A.; Cournapeau, D.; Brucher, M.; Perrot, M.; Duchesnay, É. Scikit-Learn: Machine Learning in Python. *J. Mach. Learn. Res.* **2011**, *12* (85), 2825–2830.